Food Chemistry: X 22 (2024) 101297

Contents lists available at ScienceDirect

Food Chemistry: X

journal homepage: www.sciencedirect.com/journal/food-chemistry-x

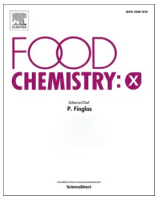

Label-free Raman imaging for screening of anti-inflammatory function food

Qi Zeng [a,b,c], Yangyao Peng [a,b], Xianzhen Zhou [a,b], Jiaojiao Zhang [a,b], Yuhang Yang [a,b], Xinyi Xu [a,b,c], Bin Guan [d], Yuntian Zhang [e], Xiaojia Hu [e,**], Xueli Chen [a,b,c,*]

[a] Center for Biomedical-photonics and Molecular Imaging, Xi'an Key Laboratory of Intelligent Sensing and Regulation of trans-Scale Life Information, School of Life Science and Technology, Xidian University, Xi'an, Shaanxi 710126, China
[b] Engineering Research Center of Molecular and Neuro Imaging, Ministry of Education, Xidian University, Xi'an, Shaanxi 710126, China
[c] Innovation Center for Advanced Medical Imaging and Intelligent Medicine, Guangzhou Institute of Technology, Xidian University, Guangzhou, Guangdong 510555, China
[d] Affiliated Wuxi Fifth Hospital of Jiangnan University, Wuxi Fifth People's Hospital, Wuxi 214000, China
[e] Shanghai Nature's Sunshine Health Products Co. Ltd, Shanghai 200040, China

ARTICLE INFO

Keywords:
Anti-inflammatory
Plant-based ingredient
Raman imaging technique
Coherent anti-stokes Raman scattering

ABSTRACT

Natural bioactive compounds and plant constituents are considered to have a positive anti-inflammatory effect. This study aimed to establish a screening technique for anti-inflammatory function in foods based on label-free Raman imaging. A visible anti-inflammatory analysis method based on coherent anti-Stokes Raman scattering (CARS) was established with an LPS-induced RAW264.7 cell model. Dynamic changes in proteins and lipids were determined at laser pump light wavelengths of 2956 cm^{-1} and 2856 cm^{-1}, respectively. The method was applied to a plant-based formula (JC) with anti-inflammatory activity. Q-TOF-MS and HPLC analyses revealed the main active constituents of JC as quercetin, kaempferol, L-glutamine, and sodium copper chlorophyllin. In *in vitro* and *in vivo* verification experiments, JC showed significant anti-inflammatory activity by regulating the TLR4/NF-κB pathway. In conclusion, this study successfully established a label-free and visible method for screening anti-inflammatory constituents in plant-based food products, which will facilitate the evaluation of functional foods.

1. Introduction

In modern society, involving stress, exposure to environmental toxins, and consumption of highly processed foods, there is a growing awareness of the benefits of a diet rich in plant-based foods for the prevention and, indeed, treatment of chronic diseases. Accumulating evidence supports the role of plant constituents in promoting physiological functions beyond basic nutrition (Buathong & Duangsrisai, 2023). The traditional therapeutic application of herbs and extracts has globally laid a foundation centuries ago, and the current market for plant-based functional foods, food supplements, and drugs has shown an explosive growth. Modern pharmacology provides convincing evidence to support such products, and the antioxidant and anti-inflammatory properties of plant constituents are a primary focus of study.

Inflammation is a natural immune response to stress, injury, infection, or toxic stimuli, and chronic inflammatory diseases such as metabolic syndrome, dementia, and cancer account for more than half of the total deaths worldwide. The pathogenesis of inflammation is complex, but production of nitric oxide (NO) and release of cytokines are accompanying factors widely used for the preliminary evaluation of agents with anti-inflammatory activity (Hou, Chen, Yang, & Ji, 2020). Pro-inflammatory cytokines produced by immune cells are commonly regarded as the main target for evaluation (Khan et al., 2014), and anti-inflammatory activities on macrophage cell lines are a primary mode of assessment. Measuring NO production, mRNA expression, expression of inflammatory modulators (interleukin-1β/2/5/6/8/10, tumor necrosis factor α [TNF-α], prostaglandin E2-PGE2, and others), and key proteins in macrophage cells RAW264.7, or other cell types, can provide evidence for anti-inflammatory activity *in vitro* (Gresa-Arribas et al., 2012). For *in vivo* studies, mouse, rat, and zebrafish are generally selected as animal models (Brugman, 2016; Inada, Hirota, & Shingu, 2015). Lipopolysaccharide (LPS), xylene, arachidonic acid, croton oil, dextran sulfate sodium (DSS) and 2,4,6-trinitrobenzene sulfonic acid are frequently employed to induce an inflammatory response in these models

* Corresponding author at: Center for Biomedical-photonics and Molecular Imaging, Xi'an Key Laboratory of Intelligent Sensing and Regulation of trans-Scale Life Information, School of Life Science and Technology, Xidian University, Xi'an, Shaanxi 710126, China.
** Corresponding author.
E-mail addresses: alfredxjhu@hotmail.com (X. Hu), xlchen@xidian.edu.cn (X. Chen).

https://doi.org/10.1016/j.fochx.2024.101297
Received 2 November 2023; Received in revised form 13 March 2024; Accepted 13 March 2024
Available online 16 March 2024
2590-1575/© 2024 The Authors. Published by Elsevier Ltd. This is an open access article under the CC BY-NC-ND license (http://creativecommons.org/licenses/by-nc-nd/4.0/).

(Antoniou et al., 2016; Perse & Cerar, 2012). Although these methods of inflammation evaluation are used in standard practice, their complexity and errors arising from the use of a single activity test can have serious drawbacks (D. Zhang, Wang, Slipchenko, & Cheng, 2014).

The ability to obtain spatiotemporal function information from biological systems in a label-free manner can solve many problems currently emerging in activity screening applications (Camp & Cicerone, 2015). A real-time, visible monitoring technique that provides a comprehensive evaluation index of both pharmacodynamic and mechanism information would be highly desirable for development (Tan et al., 2022; D. Zhang et al., 2014). Coherent Raman scattering (CRS) microscopy provides feasibility for noninvasive label-free visualization of endogenous biomolecules in biological samples, by detecting vibrations of chemical bonds within molecules (Shi et al., 2023). Unlike the spontaneous Raman scattering, CRS utilizes a nonlinear process to enhance the Raman signal for fast imaging. As a CRS technology, coherent anti-Stokes Raman scattering (CARS) microscopy offers high spatial resolution and sufficient chemical contrast without single photon fluorescence; thus, it has been successfully applied in the field of life sciences (Steuwe et al., 2014). Many of the applications of CARS microscopy focus on imaging lipids or lipid droplets (LDs) to study their metabolism under certain conditions(Borek-Dorosz et al., 2022; C. Zhang & Boppart, 2020). LDs play a crucial role in lipid metabolism and cell signaling, and the dysregulation of lipid metabolism can lead to many diseases. By acquiring CARS images at different wavenumbers, more detailed components such as LDs, proteins, and DNA can be visualized inside cells or tissues(Fung & Shi, 2020).

Based on the label-free CARS imaging technique, this study established a method for screening compounds with anti-inflammatory activity; And a plant-based formula (JC) with the potential anti-inflammatory activity were evaluate. In the context of a network pharmacological analysis, *in vitro* and *in vivo* tests were undertaken on JC to verify its anti-inflammatory activity and to explore the mechanisms involved. Thus, this study established an effective label-free Raman imaging technique for screening anti-inflammatory function in foods.

2. Materials and methods

2.1. Materials

Dulbecco's modified Eagle medium (DMEM) and fetal bovine serum (FBS) were purchased from HyClone (Logan, UT, USA). 100× Penicillin, streptomycin (P/S), and NO product kit were purchased from Sangon Biotech (Shanghai, China). Trypsin (0.25%) and Nuclear and Cytoplasmic Protein Extraction Kit were obtained from Beyotime (Shanghai, China). Dimethyl sulfoxide and MTT were purchased from Sigma–Aldrich (St. Louis, MO, USA). Enzyme-linked immunosorbent assay (ELISA) kits for mouse interleukin (IL)-1β and IL-10 were purchased from NeoBioscience (Shenzhen, China). LPS was sourced from Macklin (Shanghai, China). RNA extraction kit was purchased from Yuduo (Shanghai, China). SYBR Green polymerase chain reaction (PCR) kit and RevertAid First Strand cDNA Synthesis Kit were purchased from Thermo (Waltham, MA, USA). Bicinchoninic acid (BCA) Protein Assay Kit was obtained from Biosharp (Anhui, China). Polyvinylidene difluoride (PVDF) membranes were purchased from Millipore (Darmstadt, Germany). Phosphate-buffered saline (PBS) was sourced from Puhe (Wuxi, China). The primary antibodies (NF-Kb p65, TBP) used for western blot analyses were purchased from Abcam (Cambridge, London, UK); PKC-γ and GAPDH were sourced from HuaBio (Hangzhou, China) and Proteintech (Chicago, IL, USA), respectively. The JC was obtained from Nature's Sunshine Products Inc. (Shanghai, China).

2.2. LPS-induced cell model and CARS imaging

RAW264.7 cell line was purchased from Chinese Tissue Culture Collections (CTCC) and cultured in DMEM (supplemented with 10% FBS and 1% P/S) in a humidified incubator at 5% CO_2 and 37 °C.

Four groups were established for the CARS-based anti-inflammatory assay: (1) Control group (untreated cell lines); (2) LPS group (LPS), wherein the final concentration of LPS was 1 μg/mL; (3) LPS + quercetin group (LQ), wherein the final concentrations of LPS and quercetin were 1 μg/mL and 2 μg/mL, respectively; (4) LPS + JC group (LJC), wherein the final concentration of LPS and JC were 1 μg/mL and 16 μg/mL, respectively. Stock solutions of LPS, quercetin, and JC were prepared to 1.0, 1.0, and 32.2 mg/mL, respectively, in PBS solution, and samples were diluted to the appropriate concentration for each experiment.

The wave number range for CARS was deduced as follows. Based on a network pharmacology calculation and a literature review, the interacting proteins and signaling pathways of the main constituents could be summarized by AKT-related pathways. The amino acid sequences of each protein based on their quantity from highest to lowest were sorted, and the amino acids in the top two ranks were selected. The side chain group structures of these amino acids were used as the criteria for defining the CARS wavenumber range.

The CARS sample preparation process was as follows. First, a double-sided tape was applied onto a glass slide, and a sample space (approx.10 mm) was hollowed out at the center of the tape. Subsequently, a small amount of culture medium containing cells (1–2 μL) was added into the sample space. A piece of cover glass was overlaid to ensure that the droplets did not touch the double-sided tape. Finally, the upper and lower sides of the sample were adhered to the water mirror and the oil mirror, respectively, to collect the CARS image. Cells were evaluated after 24 and 48 h. A supercontinuum fiber laser, serving as the pump beam for CARS signal excitation, provided a pulse train with a repetition rate of 40 MHz and an adjustable output between 400 and 2400 nm. The total power and pulse duration were 4 W and 58 ps, respectively. Another pulse train was employed as the Stokes beam, with the excitation source being centered at 1064 nm, a pulse duration of 186 fs, and a pulse power of 1.1 W. The optical system structure and parameters were designed according to a published study (Zhang et al., 2022). Data processing was performed with ImageJ (version v1.52i). The intensity ratio of bright and dark areas, assessed by manual selection, was used as an evaluation index, and the calculation methods were in accordance with the built-in analysis tool. The signal-to-noise ratio (SNR) was also employed as an evaluation index.

2.3. Network pharmacology analysis

2.3.1. Predicting potential targets of JC

Targets of JC were searched from TCMSP database (screened based on OB ≥ 30%, DL ≥ 0.18, https://old.tcmsp-e.com/tcmsp.php) and Swiss Target Prediction System (http://www.swisstargetprediction.ch/, accessed on August 12, 2022). Duplicates were removed, and information from the UniProt database (https://www.uniprot.org/, accessed on June 30, 2022) was used to standardize the target names into gene names.

2.3.2. Inflammation-associated target genes

The keyword "resist inflammation" was inputted into the GeneCards database (https://www.genecards.org/, accessed on August 8, 2022) to search for target genes. Plant formula and inflammation-associated targets genes were imported into the Venny 2.1 online mapping tool platform (https://bioinfogp.cnb.csic.es/tools/venny/index.html) to obtain intersecting genes.

2.3.3. Drug–target–disease network construction

Cytoscape 3.9.1 software was applied for visual analyses of the drug–target–disease network using the Network Analyzer plug-in for network topology analysis to obtain degree values and betweenness centrality.

2.3.4. Protein–protein interaction network construction

Protein–protein interaction (PPI) network data were obtained from the STRING online database (http://cn.string-db.org, accessed on August 12, 2022) by inputting the aforementioned intersecting target genes. The parameter "Organisms" was limited to "*Homo sapiens*," and the medium confidence score was set at >0.900, with the disconnected nodes having removed. The PPI network was visualized using Cytoscape.

2.3.5. Enrichment of gene ontology and Kyoto encyclopedia of genes and genomes pathways

The Metascape database (http://metascape.org, accessed on August 13, 2022) was utilized to analyze the Gene Ontology (GO) and Kyoto Encyclopedia of Genes and Genomes (KEGG) pathway enrichments. The top 20 data in each enrichment analysis were further *v*isualized with an online platform for data analysis and visualization (https://www.bioinformatics.com.cn, last accessed on August 13, 2022).

2.4. Quadrupole–time of flight–mass spectrometry analysis

An Agilent 1290 Infinity UHPLC system was used for this analysis (Agilent 6545 Quadrupole–Time of Flight–Mass Spectrometer with a dual jet stream electrospray ion source; Agilent, USA). An Endeavorsil 1.8 μm C18 column (50 × 2.1 mm) was employed for detecting both positive and negative modes. The binary gradient elution system consisted of (A) 0.1% (*v*/v) formic acid dissolved in acetonitrile and (B) 0.1% (v/v) formic acid dissolved in water. Separation was achieved using the following gradient: 0 min, 5% A; 0.5 min, 5% A; 5 min, 30% A; 9.5 min, 90% A; 9.75 min, 5% A; and 12 min, 5% A. The flow rate was set at 0.3 mL/min at a column temperature of 40 °C, and all sample injection volumes were 5 μL. The mass range was from *m/z* 100 to 1200.

The mass spectrometer operated was as follows: spray voltage, 4000 *V* in positive mode and 3500 V in negative mode; gas temperature, 350 °C; drying gas flow rate, 8 L/min; nebulizer pressure, 35 psig; and fragmentor, 175 V (115 V for Glucoraphanin). Data were collected *via* Agilent MassHunter workstation software and evaluated by MassHunter qualitative and quantitative analysis software.

2.5. HPLC analysis

A high-performance liquid chromatography (HPLC) system was used (SPD-2 A UV detector, CTO-10AS column oven, LC-2AT pump; Shimadzu, Japan). An Inertsil ODS-SP C18 (4.6 × 250 nm, 5 μm) column was employed. The binary gradient elution system consisted of (A) chromatography grade methanol and (B) 0.05 mol/L potassium dihydrogen phosphate solution. Separation of the components was achieved by using the following gradient: 0 min, 100% B; 10 min, 95% B; 25 min, 80% B; 30 min, 100% B; flow rate of 1 mL/min and a column temperature of 30 °C. Separation was carried out using the following gradient. All samples were injected at a volume of 20 μL (per injection) during the assay, and detection was performed at a wavelength of 235 nm.

2.6. In vitro experiments

2.6.1. Cell viability assay

RAW264.7 cells in the logarithmic growth phase were uniformly seeded into 96-well plates at a density of 1×10^5 cells/well. After 24-h incubation, according to the double-dilution method, the control group and JC groups (0.5, 1.01, 2.01, 4.02, 8.05, 16.1, and 32.2 μg/mL) were set up with three replicate wells. The MTT method was used to measure the optical density (OD) values in different wells using a microplate analyzer at 490 nm. The survival rate of RAW264.7 cells was calculated according to the following formula:

$$survival\ rate = \frac{OD_{drug} - OD_{blank}}{OD_{control} - OD_{blank}} \times 100\%$$

2.6.2. Nitric oxide assay

RAW264.7 cells (2×10^5 cells/well) were seeded in 12-well plates and incubated for 24 h. Cells were treated with different concentrations (0, 8, 16, 32, and 64 μg/mL) for JC and 1 μg/mL LPS for 24, 48, and 72 h. The medium was collected at each time point to determine NO production.

2.6.3. Reverse transcription–polymerase chain reaction assay

The groups were set as control group, LPS group (1 μg/mL LPS), and JC group (16 μg/mL W and 1 μg/mL LPS). The preparation of the cells and tissues was carried out according to the kit instructions. mRNA was extracted from each group using the RNAsimple total RNA Kit. cDNA was synthesized by reverse transcription using the PrimeScript™ 1st Strand cDNA Synthesis Kit. A 20-μL Real-time PCR system was established, and cDNA was reverse transcribed by real-time fluorescent quantitative PCR assay. The mRNA expression profiles were normalized to that of GAPDH. The primers used for this assay were as follows: GAPDH forward 5′-GGTGAAGGTCGGTGTGAACG-3′ and reverse 5′-CTCGCTCCTGGAAGATGGTG-3′; TLR2 forward 5′-TGGTTCCCTGCTCGTTCT-3′ and reverse 5′-CTCAAATGATTCTGGCTC-3′; TLR4 forward 5′-GAGCCGTTGGTGTATCTT-3′ and reverse 5′'-GTTGCCGTTTCTTGTTCT-3′; IL-6 forward 5′-ATGATGGATGCTACCAAACT-3′ and reverse 5′-TATCTCTCTGAAGGACTCTG-3′; IL-1β forward 5′-TGTGTAATGAAAGACGG-3′ and reverse 5′-TGTGAGGTGCTGATGTA-3′; TNF-α forward 5′-CGTCGTAGCAAACCACC3′ and reverse 5′-CCCTTGAAGAGAACCTG-3′.

2.6.4. Enzyme-linked immunosorbent assay (ELISA)

RAW264.7 cells growing on 12-well plates were divided into three groups. In addition to the control group, RAW264.7 cells were treated with LPS (1 μg/mL) in the presence or absence of JC (16 μg/mL) for 24, 48, and 72 h. ELISA kits were used to assess the secretion of IL-1β and IL-10 from the supernatants of cell cultures using the ELISA Kit.

2.6.5. Western blot analysis

The cells (5×10^5 cells/well) were cultured in 60-mm culture dishes, and the treatment method was the same as that of ELISA. After incubating the cells for 72 h, the cellular nuclear and cytoplasmic proteins were extracted using the Nuclear and Cytoplasmic Protein Extraction Kit. Total protein concentration was detected according to the BCA method, and the standard curve was constructed according to the following formula:

$$A = 0.5644C(mg/ml) + 0.0239$$

The sodium dodecyl sulfate–polyacrylamide gel electrophoresis method was used to visualize the adhesive proteins (concentrated gel: 80 *V*, separator gel: 120 V). The gel was transferred onto a PVDF membrane and was blocked with confining liquid for 1 h (5% skimmed milk). NF-κB p65 (1:2000), PKC-γ (1:1000), TBP (1:1000), and GAPDH (1:1000) antibodies were added to the membranes and incubated overnight at 4 °C. The membranes were washed five times (10 min each time) with Tris-buffered saline with Tween 20 and incubated with the corresponding peroxidase-conjugated secondary antibody (1:5000 dilution) for 1 h at room temperature. The PVDF membranes were covered using an electrochemiluminescence kit and were photographed using a ChemiScope 5300 Pro instrument.

2.7. In vivo experiments

Thirty-six BALB/c female 4-week-old mice with bodyweight of 20.0 ± 1.0 g were purchased from Xi'an Ensiweier Biotechnology (license number: SCXK (Xiang) 2019–0004). The mice were housed in a clean, specific pathogen-free grade environment at constant temperature and humidity. All experiments were conducted under internationally accepted guidelines for laboratory animal use and care, approved by the Committee for Animal Use and Care in the Laboratory (Laboratory

Animal Ethics No. CDDEACL2022–37).

The mice were divided into three groups, as shown in Fig. 1: (1) control group ($n = 3$), wherein saline was administered intragastrically (ig); (2) DSS group ($n = 15$), wherein 600 μL of 2.5% DSS was administered three times a day from day 7 to day 14 (ig); (3) JC group ($n = 18$), wherein 650 mg/d of JC was administered from day 1 to day 44 (ig) and 2.5% DSS was added the same way as that in the DSS group from day 7 to day 14. The mental state, feeding, and daily activities of the mice were observed every day. Disease activity indices (DAIs) were recorded on days 5, 11, 23, 30, and 44. The scoring criteria for the DAI were as follows: 0 points for no weight loss, normal stool consistency, and no blood in the stool; 1 point for weight loss of 1%–5%; 2 points for weight loss of 5%–10%, semi-liquid stool, and positive occult blood in the stool; 3 points for weight loss of 10%–15%; and 4 points for weight loss >15%, loose stool, and visible blood in the stool. In the JC and DSS groups, three mice from each group were killed by cervical dislocation on days 15, 23, 30, and 44. Blood and intestinal tissue samples were collected.

Hematoxylin-eosin (HE) staining was performed to visualize the tissue structure. Colon and duodenal tissues were fixed with 4% paraformaldehyde for HE staining. The remaining colon tissues were stored in liquid nitrogen for western blot analysis. Intestinal tissues were embedded in paraffin and then sliced into 5-mm-thick sections.

2.8. Statistical analysis

Experimental results were presented as mean ± standard deviation (SD) through triplicate experiments. Statistical analysis was performed using GraphPad Prism software (GraphPad Software Inc., Avenida, CA, USA). The p values were calculated using the t-test. $p < 0.05$ was considered as statistically significant, and n.s. indicated not statistically significant. Details of each statistical analysis are provided in the figure captions.

3. Results and discussion

3.1. Construction of the CARS imaging method for anti-inflammatory assay

Fluorescent labels have been used widely for real-time imaging of biomolecule dynamics. However, because of their molecular size, fluorescent protein labels might destroy or significantly perturb the biological activities of small biomolecules (Georgakoudi & Quinn, 2012). As a chemically selective, highly sensitive, and high-speed imaging technique with submicron resolution, CARS imaging can be used to perform quantitative assessment of the metabolic activities of biomolecules (*e.g.*, lipids, proteins, and nucleic acids) in single live cells with a label-free protocol (Yue & Cheng, 2016). Thus, this study constructed a validation method for anti-inflammatory drugs based on CARS imaging.

A primary analysis of the mechanism revealed that LPS-induced inflammation can alter protein and lipid contents in cells. In the carbon-hydrogen (C-H) region, CH_3 asymmetric stretch (2956 cm^{-1}) (Corasi Ortiz, Xie, Ribbe, & Ben-Amotz, 2006), CH_3 stretching vibrations (2947 cm^{-1}) (Caspers et al., 2001), CH stretch of lipids and proteins (2931 cm^{-1}), and CH_2 symmetric stretch (2856 cm^{-1}) (Koljenović, Schut, Vincent, Kros, & Puppels, 2005) were selected by controlling the wavelength of the pump light. As shown in Fig. 2A, LPS-induced RAW264.7 cells were imaged with CARS at different wavenumbers. After 48 h since LPS-induced inflammation, RAW264.7 cells exhibited changes in the amount of intracellular substances at different wavenumber. To acquire the signal changes in a better manner, two data analysis modes were established. The first mode focused on the intensity ratio between bright and dark areas in cells, which served as a comparison between active and inactive physiological regions of the cells. The intensity ratio was calculated by using the average of three cells in the same wavenumber CARS images at different time points in each group. The second mode, based on the SNR to show changes in cellular physiological activity compared with that in the external environment, was calculated from the ratio of the mean value of the bright region to

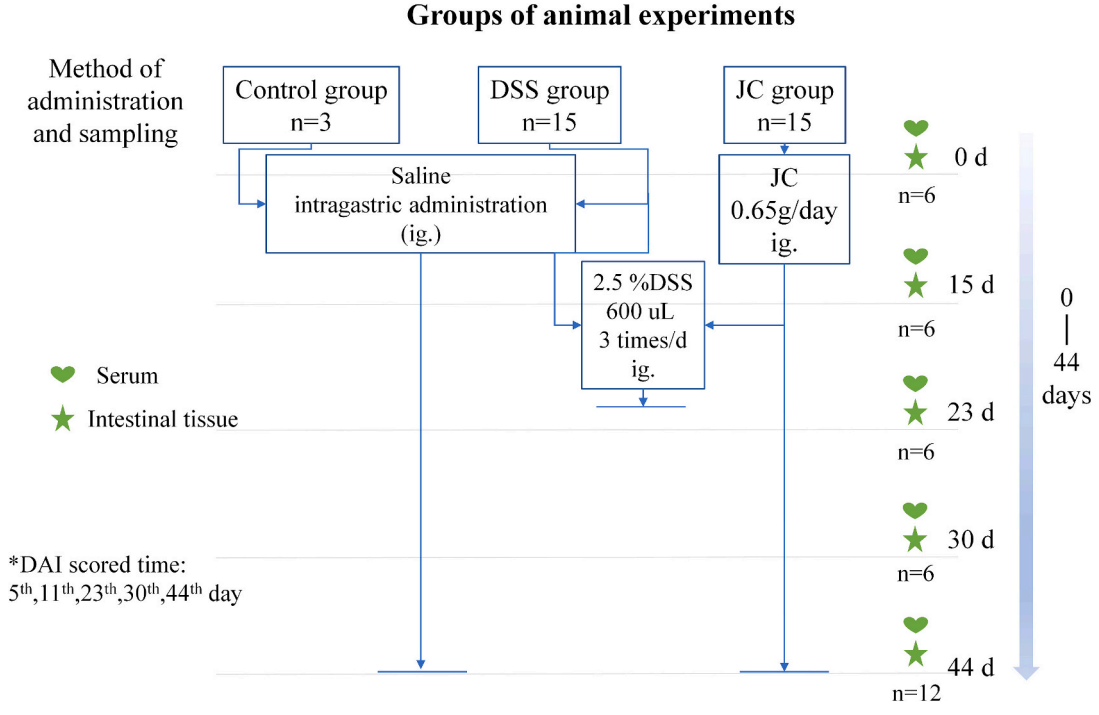

Fig. 1. Design of *in vivo* experiment.

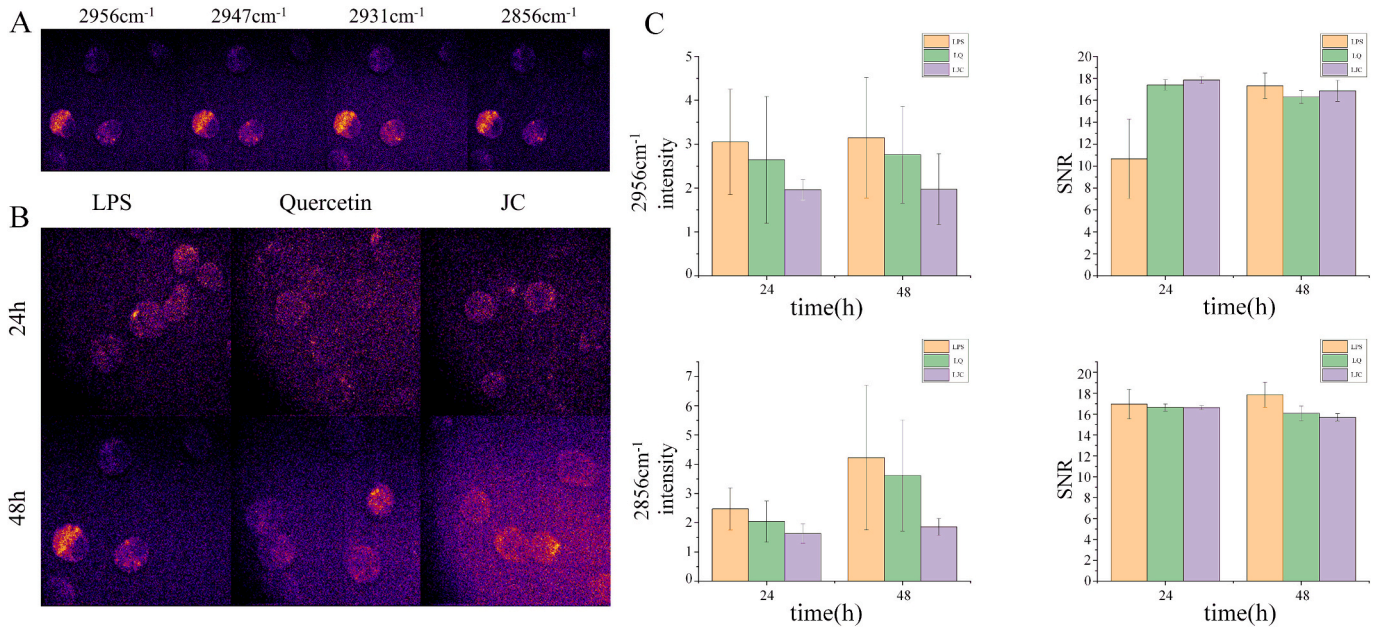

Fig. 2. Analysis of CARS imaging results. (A) CARS imaging of LPS-induced inflammation in four wavenumber ranges; (B) Distinction of RAW264.7 cells CARS imaging after different drug treatments at 24 h and 48 h and (C) Gray statistical map of intensity ratio and SNR.

the background standard deviation. The intensity ratio and SNR are shown in Table S1. From 2956 cm^{-1} to 2856 cm^{-1}, the intensity ratio presented a downward trend and the SNR remained relatively stable with no significant trend. Thus, 2956 cm^{-1} and 2856 cm^{-1} were chosen as the imaging parameters for evaluating anti-inflammatory activity.

The CARS imaging results are shown in Fig. 2B and C. Generally, the

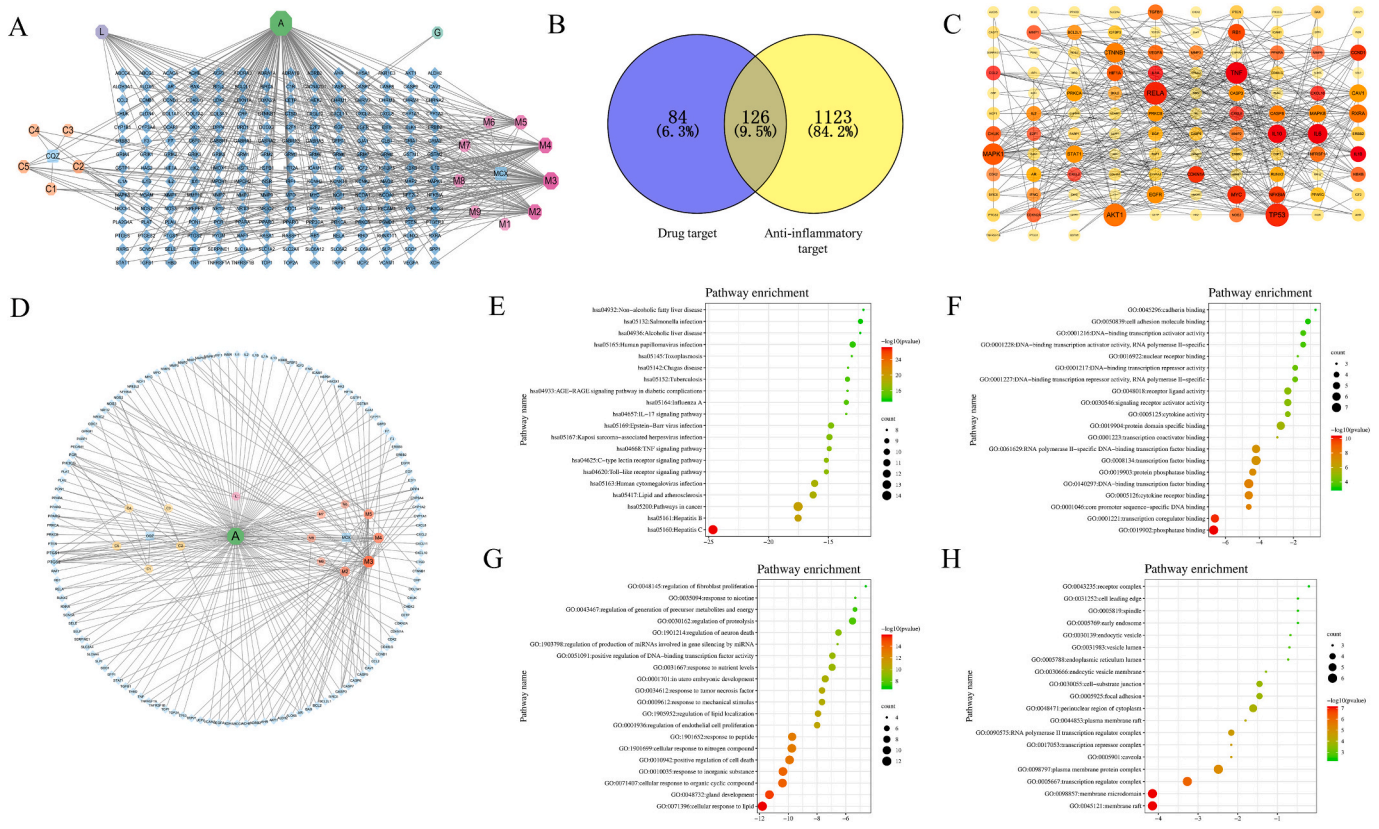

Fig. 3. Network pharmacology analysis of JC for anti-inflammatory effects. (A) Plant formula-target network; (B) Venn diagram showing the intersection of drug targets and anti-inflammatory targets; (C) PPI network of common target protein; (D) Drug−target−disease network. The blue rhombus nodes represent common targets, and the polygon node represents represent ingredients of the plant-based formula. (E) KEGG pathway analysis; (F) Molecular function analysis; (G) Biological process analysis; (H) Cellular component analysis. (For interpretation of the references to colour in this figure legend, the reader is referred to the web version of this article.)

2959 cm^{-1} spectral range was identified with protein imaging, while 2856 cm^{-1} was associated with lipid imaging. The intensity ratio of the LPS group in CARS imaging at 2959 cm^{-1} was higher than that of the LQ group, with the ratio for LJC being the lowest, and the data showed minimal changes between 24 h and 48 h time points. These results suggested that both quercetin and JC could inhibit the inflammatory effects of LPS. As for the intensity ratio at 2856 cm^{-1}, the results showed an increasing trend over time for all groups, except JC. The SNR results indicated that the CARS signal intensity showed only little variation relative to noise with the exception of that for the LPS group after 24 h. A semi-quantitative analysis of intensity ratio could better intuitively reflect the anti-inflammatory activity. The inconsistent changes between the two vibrational bands (as shown in Fig. 2C) might be attributed to two reasons: (1) the main functional groups contributing to the signals are different; and (2) the final concentration of the anti-inflammatory drugs is lower, leading to lower activity.

In conclusion, the CARS imaging results provided a compelling indication that JC might be a potential anti-inflammatory plant-based formula. The following tests were performed to confirm the anti-inflammatory activity of JC, both *in vitro* and *in vivo*.

3.2. Network pharmacology analysis

Network pharmacology analysis was carried out initially, before accurate verification experiments. After removing duplicates and standardizing target names, a total of 210 target constituents of JC were filtered from TCMSP and Swiss Target Prediction databases. As shown in Fig. 3A, the size of the blue rhombuses and polygons, corresponding to target genes and JC constituents, respectively, represents the degree value. Setting “resist inflammation” as the keyword, 1249 of 9117 inflammation-associated targets were screened from the GeneCards database, with a relevance score of >5. The 210 targets of JC were mapped with the 1249 anti-inflammation targets on a Venn diagram (Fig. 3B), identifying 126 targets with potential therapeutic effects for inflammatory conditions. A PPI network exported from the STRING database was optimized using Cytoscape to gain a better visualization and analyze the interaction of the targets (Fig. 3C) through a topology analysis. Subsequently, the node degree and betweenness centrality above the average value were used to select significant targets, including AKT1, TNF, IL-10, and MAPK1 (Table S2). Similarly, topological analysis of the drug–target–disease network identified quercetin, kaempferol, and arachidonic acid as significantly active compounds (Fig. 3D; Table S3).

These 21 significant targets were uploaded to the Metascape platform for GO and KEGG pathway enrichment analysis (Fig. 3E-H). GO enrichment analysis comprised biological process (BP), cellular component (CC), and molecular function (MF) factors. The top 20 results of the enrichment analysis with a p value of <0.01 were retrieved. The KEGG pathway enrichment analysis revealed that lipid and atherosclerosis, TNF, and hepatitis B/C pathways were all associated with the inflammatory process. The top 3 BP terms were “cellular response to lipid,” “gland development,” and “cellular response to organic cyclic compound.” Regarding the CC terms, “membrane raft,” “membrane microdomain,” and “transcription regulator complex” ranked highest. Regarding the MF terms, “phosphatase binding,” “transcription coregulator binding,” and “core promoter sequence-specific DNA binding” were the top three. The GO analysis results indicated that the targets were closely related to lipid, membrane, and gene regulation. Overall, network pharmacology analysis suggested that JC might play an active role in anti-inflammation through multiple targets and pathways.

3.3. Composition analysis of plant-based ingredients

The main components of the selected plant-based formula JC were the extracts of broccoli, *Portulaca oleracea* L. (PO), L-glutamine, sodium copper chlorophyllin, and psyllium (PS), a composition representative of plant-based supplements. Broccoli, a vegetable rich in antioxidants, has demonstrated significant health-promoting effects including antioxidant, anti-inflammatory, and anticancer effects (Ruhee & Suzuki, 2020; Syed et al., 2023). PO possesses the concomitant function of both medicine and foodstuff and acts as an antioxidant and immune-modulator of Th1 and Th2 responses (Rahimi, Ajam, Rakhshandeh, & Askari, 2019). PS, comprising 10%–30% of the JC composition, is a soluble dietary fiber and intestinal transit modulator and exerts other benefits for metabolic syndrome (Hussain, Muhammad, Jantan, & Bukhari, 2016). Meanwhile, L-glutamine and sodium copper chlorophyllin have well-documented antioxidant, anti-inflammatory, and antibacterial activities (Durante, 2019). The results of Q-TOF-MS revealed the presence of quercetin and L-glutamine (Fig. S1), and sodium copper chlorophyllin was identified by HPLC analysis (Fig. S2). Thus, these results are consistent with those of network pharmacology.

3.4. In vitro verification

In the cell growth inhibition evaluation, JC exhibited no significant toxicity effect on RAW264.7 in the concentration range of 0–16.1 μg/mL, while a concentration of 32.2 μg/mL showed slight cell growth inhibitory activity (Fig. 4A). Hence, the concentration selected for subsequent *in vitro* tests was 16.1 μg/mL. As shown in Fig. 4B, JC inhibited the LPS-induced NO expression in a dose-dependent manner, indicating its potential anti-inflammatory activity. Further study focused on the anti-inflammatory mechanism of JC and the correlation factors for the high expression signal in CARS imaging.

Toll-like receptors (TLR) play a crucial role in the detection of microbial infection and the activation of inflammatory and antimicrobial innate immune responses (Duan, Du, Xing, Wang, & Wang, 2022). The expression levels of TLR2 and TLR4 were markedly elevated in LPS-induced RAW264.7 cells. JC significantly reduced TLR2 and TLR4 expression (Fig. 4C-D). TLR2 has a specific role in recognizing different types of lipopeptides derived from bacteria or parasites (Marks, Cho, Stickling, & Reynolds, 2021). TLR4 can recognize LPS to activate MyD88 pathways, resulting in the production of proinflammatory cytokines (Bruning, Coller, Wardill, & Bowen, 2021). The expression of TLR2 and TLR4 mRNA was examined in LPS-induced RAW264.7 cells, and these experimental results were consistent with those of previous research (Liu et al., 2001; Qi, Cui, Liu, Luo, & Wang, 2020). Therefore, JC could inhibit inflammation by regulating TLR4 and TLR2 expression.

To further verify the activity of JC, the expression of IL-1β and IL-10 was measured through ELISA. As shown in Fig. 4E-F, LPS upregulated the expression of IL-1β and IL-10 compared with that in the control group. Notably, after treatment with JC, IL-1β expression was downregulated, while IL-10 expression was upregulated. Cytokines, as key modulators of inflammation, are important anti-inflammatory targets . LPS-induced macrophages release various pro-inflammatory cytokines including IL-1β, IL-6, TNF-α, and COX-2. IL-1β is a potent pro-inflammatory cytokine, originally identified as an endogenous pyrogen (Turner, Nedjai, Hurst, & Pennington, 2014). IL-10 plays an important role in anti-inflammation by controlling essential metabolic pathways, including mTOR signaling (Ip, Hoshi, Shouval, Snapper, & Medzhitov, 2017). Thus, JC downregulated the expression of IL-1β to exert anti-inflammatory effects while upregulating the expression of IL-10 to prevent the generation of cytokine storms.

A western blot assay was performed to unravel the anti-inflammatory mechanism of JC. As shown in Fig. 4G-J, LPS stimulated upregulated expression of PKC-γ and nuclear and cytoplasmic NF-κB p65 proteins. However, JC could inhibit this effect, downregulating the expression of these proteins. PKC is a family of serine-threonine protein kinase isoenzymes that play an important role in cellular signal transduction, cell growth, and cell proliferation (Salonen et al., 2006; Yuan et al., 2019). The activation of the PKC pathway plays a key role in the regulation of host defense and inflammation through the NF-κB signaling pathway (Fu et al., 2019). NF-κB regulates the expression of

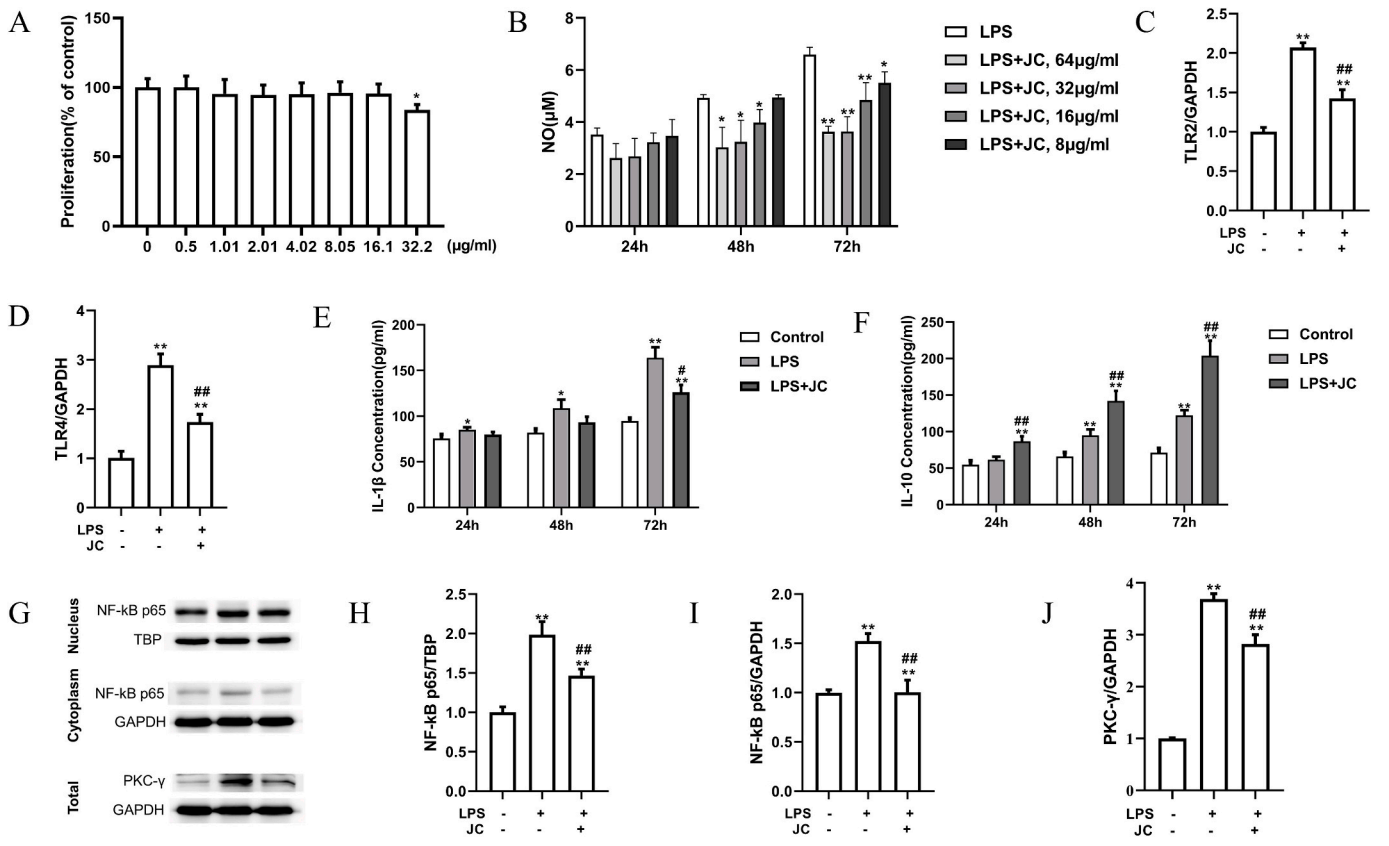

Fig. 4. Validation of the anti-inflammatory effect of JC *in vitro*. (A) Cell growth inhibition of JC on RAW264.7 cell line; (B) Effect of JC on NO production in LPS-induced RAW264.7 cells for 24 h, 48 h, and 72 h; (C)-(D) Effect of JC on the expression of mRNA levels of TLR2 (C) and TLR4 (D) induced by LPS in RAW264.7 cells; (*E*)-(F) Results of JC on the production of IL-1β (E) and IL-10 (F) in LPS-induced RAW264.7 cells; (G) western blotting results; (H)-(J) Grayscale quantitative histogram of western blotting, (H) NF-κB p65 in nucleus; (I) cytoplasm; and (J) PKC-γ. Values are presented as mean ± standard deviation ($n = 3$), $^{*}p < 0.05$, $^{**}p < 0.01$ *versus* control group, #p < 0.05, ##p < 0.01 *versus* only LPS treatment group.

pro-inflammatory genes such as iNOS and COX-2 and mediates the production of pro-inflammatory cytokines including IL-1β, IL-6, and TNF-α (Li et al., 2019). JC can inhibit LPS-mediated activation of NF-κB by suppressing p65 nuclear translocation. Generally, JC might exert an anti-inflammatory effect by modulating PKC-γ/NF-κB signaling pathways. These results are also consistent with those of network pharmacology.

In the CARS-based visual screening, the highlighted signals observed were mainly distributed on the periphery of the LPS-induced RAW264.7 cells. LPS would activate cell membrane receptor proteins (LPS-binding protein [LBP]), leading to inflammation and the expression of inflammatory factors (Fig. S3) (Ciesielska, Matyjek, & Kwiatkowska, 2021). In this study, CARS imaging at 2856 cm^{-1} and 2956 cm^{-1} recorded the LPS-induced signal enhancement of proteins on the cell membrane. Combined with the mechanism of LPS, the signals might be a comprehensive index of LBP and TLR. This hypothesis is supported by the following downstream pathway analysis results from RT-PCR, ELISA and western blotting. Hence, CARS provides a visual assessment of integral cellular inflammation and is a powerful tool for the evaluation of drug activity.

3.5. *In vivo* verification

The *in vivo* verification was based on a 44-day mouse experiment (Fig. 1). As shown in Table 1, the DAI results indicated that the DSS group had a significant reduction in weight and other related effects due to DSS-induced ulcerative colitis. The DAI scores of the JC group on days 23 and 30 were lower than those of the DSS group, demonstrating the intestinal protective activity of JC. Although three mice were killed at each time point, individual differences affecting the DAI score cannot be excluded.

Table 1
Disease activity index score.

Group	Day 5	Day 11	Day 23	Day 30	Day 44
BALB/C	0	0	0.33	0.67	0.67
DSS + physiological saline	0	0.07	2.6	0.83	0
DSS + JC	0	0.35	1.1	0.14	0.5

Note: Data are presented as mean.

RT-PCR results of intestinal tissues showed that the expression levels of TNF-α, IL-1β, and IL-6 significantly increased after DSS intervention compared with those of the control group. However, under the effect of JC, the expression levels of IL-1β and IL-6 were noticeably downregulated on day 30 after the DSS intervention, and the TNF-α expression level decreased by the end of day 23 (Fig. 5A). According to HE staining (Fig. 5B), the number of intestinal glands in the control group was normal, and the structure of the mucosal layer was complete with a tight arrangement of the submucosal layer. In the DSS group, necrosis of the intestinal glands, detachment of the epithelium from the mucosal layer, incomplete villus structure, disordered arrangement of the submucosal layer, and dissolution of the muscle layer were observed. Moreover, compared with the colon, jejunum lesions were more severe. The structure of the intestine in the JC group was complete and showed a better appearance than that of the DSS group. Therefore, it can be deduced that JC can prevent the occurrence of inflammatory lesions.

However, there remain certain disadvantages worthy of further investigation. The CARS imaging method could not clearly reveal

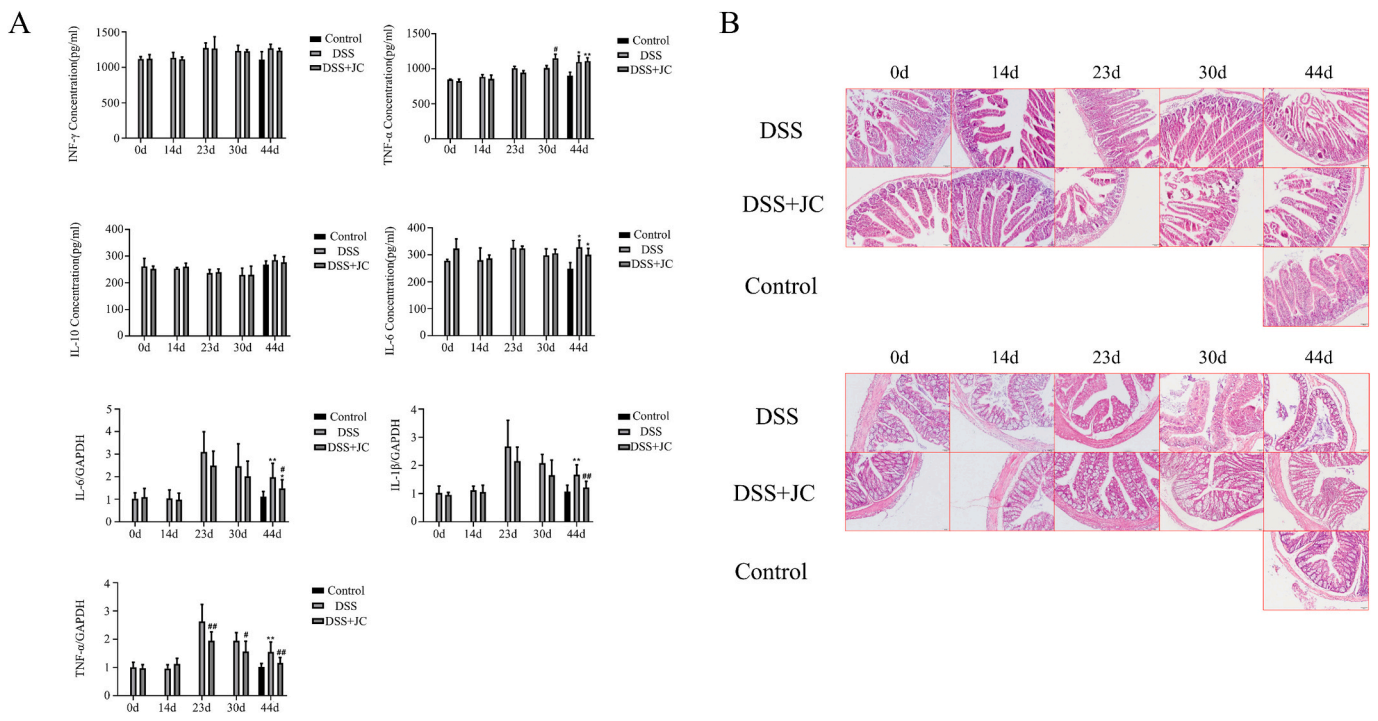

Fig. 5. Results of *in vivo* verification. (A) Mouse intestinal tissues: RT-PCR assay of TNF-α, IL-1β, and IL-6; (B) Mouse intestinal tissue section analysis.

intracellular protein or lipids in the anti-inflammatory model. This may, in part, be attributed to the detection limit and resolution of this method. Indeed, quantitative analysis of total protein showed that the expression of total proteins in the JC group was lower than that of the LPC group. However, inconsistent with the intensity quantitative analysis of CARS at 2959 cm^{-1}, the total protein content in LJC group was higher than that in LQ group (Fig. S4). This method could capture inflammatory protein expression; therefore, its specificity should be investigated. Indeed, the label-free Raman imaging techniques reflected the metabolic changes in proteins and lipids in tissues and cells with a high resolution and sensitivity (C. Zhang, Zhang, & Cheng, 2015). Thus, combining with other suitable models, CARS and similar CRS techniques could be applied in other pharmacology evaluation.

4. Conclusion

In summary, this study established a visible, label-free method for screening anti-inflammatory agents, JC may have the potential to serve as a natural functional food with inflammatory effects. The results confirmed that JC exhibited an anti-inflammatory effect in both LPS-induced inflammation in macrophages and DSS-induced mouse colitis models. The chemical components of JC mainly contain quercetin, kaempferol, L-glutamine, and sodium copper chlorophyllin. Moreover, quercetin and kaempferol might contribute to reducing inflammatory cytokine production by regulating PKC-γ/NF-κB signaling pathways. Although CARS imaging technology can facilitate visualization of the internal components in cells or tissues in a noninvasive and label-free manner, the non-resonant background of CARS may hinder the precise detection of subtle changes in cells under external interference. In future research, our research group envisions that employing other CRS techniques will improve imaging quality and provide more additional indices to facilitate further differential analysis. This label-free Raman imaging method can reveal the changes in the metabolic environment and chemical substances, possessing great potential for this application.

CRediT authorship contribution statement

Qi Zeng: Data curation, Formal analysis, Funding acquisition, Investigation, Methodology, Validation, Visualization, Writing – original draft, Writing – review & editing. **Yangyao Peng:** Data curation, Investigation, Software, Visualization, Writing – original draft. **Xianzhen Zhou:** Methodology, Software, Writing – original draft, Writing – review & editing. **Jiaojiao Zhang:** Data curation, Methodology. **Yuhang Yang:** Formal analysis, Writing – original draft. **Xinyi Xu:** Writing – original draft, Project administration, Funding acquisition. **Bin Guan:** Project administration, Data curation. **Yuntian Zhang:** Project administration, Data curation. **Xiaojia Hu:** Formal analysis, Conceptualization, Funding acquisition, Investigation, Project administration, Resources. **Xueli Chen:** Funding acquisition, Supervision, Visualization, Writing – review & editing.

Declaration of competing interest

The authors declare that they have no known competing financial interests or personal relationships that could have appeared to influence the work reported in this paper.

Data availability

Data have already been included.

Acknowledgments

This work was supported in part by the Key Research and Development Program of Shaanxi (2021ZDLSF04-05); the National Natural Science Foundation of China (62275210, 32101115); the National Young Talent Program; the Shaanxi Science Fund for Distinguished Young Scholars (2020JC-27); the Shaanxi Young Top-notch Talent Program. We would like to thank MogoEdit (https://www.mogoedit.com) for its English editing during the preparation of this manuscript.

Appendix A. Supplementary data

Supplementary data to this article can be found online at https://doi.org/10.1016/j.fochx.2024.101297.

References

Antoniou, E., Margonis, G. A., Angelou, A., Pikouli, A., Argiri, P., Karavokyros, I., … Pikoulis, E. (2016). The TNBS-induced colitis animal model: An overview. *Annals of Medicine and Surgery, 11*, 9–15. https://doi.org/10.1016/j.amsu.2016.07.019

Borek-Dorosz, A., Grosicki, M., Dybas, J., Matuszyk, E., Rodewald, M., Meyer-Zedler, T., … Baranska, M. (2022). Identification of inflammatory markers in eosinophilic cells of the immune system: Fluorescence, Raman and CARS imaging can recognize markers but differently. *Cellular and Molecular Life Sciences, 79*(1). https://doi.org/10.1007/s00018-021-04058-4. Article 52.

Brugman, S. (2016). The zebrafish as a model to study intestinal inflammation. *Developmental and Comparative Immunology, 64*, 82–92. https://doi.org/10.1016/j.dci.2016.02.020

Bruning, E. E., Coller, J. K., Wardill, H. R., & Bowen, J. M. (2021). Site-specific contribution of toll-like receptor 4 to intestinal homeostasis and inflammatory disease. *Journal of Cellular Physiology, 236*(2), 877–888. https://doi.org/10.1002/jcp.29976

Buathong, R., & Duangsrisai, S. (2023). Plant ingredients in Thai food: A well-rounded diet for natural bioactive associated with medicinal properties. *PeerJ, 11*. https://doi.org/10.7717/peerj.14568. Article e14568.

Camp, C. H., & Cicerone, M. T. (2015). Chemically sensitive bioimaging with coherent Raman scattering. *Nature Photonics, 9*(5), 295–305. https://doi.org/10.1038/Nphoton.2015.60

Caspers, P. J., H. A. B, Puppels, G. J., Lucassen, G. W., & Carter, E. A. (2001). *In vivo* confocal Raman microspectroscopy of the skin: Noninvasive determination of molecular concentration profiles. *Journal of Investigative Dermatology, 116*(3), 434–442. https://doi.org/10.1046/j.1523-1747.2001.01258.x

Ciesielska, A., Matyjek, M., & Kwiatkowska, K. (2021). TLR4 and CD14 trafficking and its influence on LPS-induced pro-inflammatory signaling. *Cellular and Molecular Life Sciences, 78*(4), 1233–1261. https://doi.org/10.1007/s00018-020-03656-y

Corasi Ortiz, D. Z., Xie, Y., Ribbe, A. E., & Ben-Amotz, D. (2006). Validation of the drop coating deposition Raman method for protein analysis. *Analytical Biochemistry, 353*(2), 157–166. https://doi.org/10.1016/j.ab.2006.03.025

Duan, T. H., Du, Y., Xing, C. S., Wang, H. Y. Y., & Wang, R. F. (2022). Toll-like receptor signaling and its role in cell-mediated immunity. *Frontiers in Immunology, 13*. https://doi.org/10.3389/fimmu.2022.812774. Article 812774.

Durante, W. (2019). The emerging role of l-glutamine in cardiovascular health and disease. *Nutrients, 11*(9). https://doi.org/10.3390/nu11092092. Article 2092.

Fu, S. Y., Xiong, R. P., Peng, Y., Zhang, Z. H., Chen, X., Zhao, Y., … Li, P. (2019). PKC mediates LPS-induced IL-1 beta expression and participates in the pro-inflammatory effect of A(2A)R under high glutamate concentrations in mouse microglia. *Neurochemical Research, 44*(12), 2755–2764. https://doi.org/10.1007/s11064-019-02895-1

Fung, A. A., & Shi, L. Y. (2020). Mammalian cell and tissue imaging using Raman and coherent Raman microscopy. *Wiley Interdisciplinary Reviews. Systems Biology and Medicine, 12*(6). https://doi.org/10.1002/wsbm.1501. Article e1501.

Georgakoudi, I., & Quinn, K. P. (2012). Optical imaging using endogenous contrast to assess metabolic state. *Annual Review of Biomedical Engineering, 14*, 351–367. https://doi.org/10.1146/annurev-bioeng-071811-150108

Gresa-Arribas, N., Vieitez, C., Dentesano, G., Serratosa, J., Saura, J., & Sola, C. (2012). Modelling Neuroinflammation *in vitro*: A tool to test the potential neuroprotective effect of anti-inflammatory agents. *PLoS One, 7*(9). https://doi.org/10.1371/journal.pone.0045227. Article e45227.

Hou, C. Y., Chen, L. L., Yang, L. Z., & Ji, X. L. (2020). An insight into anti-inflammatory effects of natural polysaccharides. *International Journal of Biological Macromolecules, 153*, 248–255. https://doi.org/10.1016/j.ijbiomac.2020.02.315

Hussain, M. A., Muhammad, G., Jantan, I., & Bukhari, S. N. A. (2016). Psyllium Arabinoxylan: A versatile biomaterial for potential medicinal and pharmaceutical applications. *Polymer Reviews, 56*(1), 1–30. https://doi.org/10.1080/15583724.2015.1078351

Inada, T., Hirota, K., & Shingu, K. (2015). Intravenous anesthetic propofol suppresses prostaglandin E-2 and cysteinyl leukotriene production and reduces edema formation in arachidonic acid-induced ear inflammation. *Journal of Immunotoxicology, 12*(3), 261–265. https://doi.org/10.3109/1547691x.2014.938874

Ip, W. K. E., Hoshi, N., Shouval, D. S., Snapper, S., & Medzhitov, R. (2017). Anti-inflammatory effect of IL-10 mediated by metabolic reprogramming of macrophages. *Science, 356*(6337), 513–519. https://doi.org/10.1126/science.aal3535

Khan, N., Khymenets, O., Urpi-Sarda, M., Tulipani, S., Garcia-Aloy, M., Monagas, M., … Andres-Lacueva, C. (2014). Cocoa polyphenols and inflammatory markers of cardiovascular disease. *Nutrients, 6*(2), 844–880. https://doi.org/10.3390/nu6020844

Koljenović, S., Schut, T. B., Vincent, A., Kros, J. M., & Puppels, G. J. (2005). Detection of meningioma in dura mater by Raman spectroscopy. *Analytical Chemistry, 77*(24), 7958–7965. https://doi.org/10.1021/ac0512599

Li, F., Song, X., Su, G., Wang, Y., Wang, Z., Qing, S., Jia, J., Wang, Y., Huang, L., Zheng, K., & Wang, Y. (2019). AT-533, a Hsp90 inhibitor, attenuates HSV-1-induced inflammation. *Biochemical Pharmacology, 166*, 82–92. https://doi.org/10.1016/j.bcp.2019.05.003

Liu, Y., Wang, Y., Yamakuchi, M., Isowaki, S., Nagata, E., Kanmura, Y., Kitajima, I., & Maruyama, I. (2001). Upregulation of toll-like receptor 2 gene expression in macrophage response to peptidoglycan and high concentration of lipopolysaccharide is involved in NF-kappa b activation. *Infection and Immunity, 69*(5), 2788–2796. https://doi.org/10.1128/IAI.69.5.2788-2796.2001

Marks, K. E., Cho, K., Stickling, C., & Reynolds, J. M. (2021). Toll-like receptor 2 in autoimmune inflammation. *Immune Network, 21*(3). https://doi.org/10.4110/in.2021.21.e18. Article e18.

Perse, M., & Cerar, A. (2012). Dextran sodium sulphate colitis mouse model: traps and tricks. *BioMed Research International, 2012*. https://doi.org/10.1155/2012/718617. Article 718617.

Qi, S. R., Cui, Y. J., Liu, J. X., Luo, X., & Wang, H. F. (2020). *Lactobacillus rhamnosus* GG components, SLP, gDNA and CpG, exert protective effects on mouse macrophages upon lipopolysaccharide challenge. *Letters in Applied Microbiology, 70*(2), 118–127. https://doi.org/10.1111/lam.13255

Rahimi, V. B., Ajam, F., Rakhshandeh, H., & Askari, V. R. (2019). A pharmacological review on *Portulaca oleracea* L.: focusing on anti-inflammatory, anti- oxidant, immuno-modulatory and antitumor activities. *Journal of Pharmacopuncture, 22*(1), 7–15. https://doi.org/10.3831/KPI.2019.22.001

Ruhee, R. T., & Suzuki, K. (2020). The integrative role of Sulforaphane in preventing inflammation, oxidative stress and fatigue: A review of a potential protective phytochemical. *Antioxidants, 9*(6). https://doi.org/10.3390/antiox9060521. Article 521.

Salonen, T., Sareila, O., Jalonen, U., Kankaanranta, H., Tuominen, R., & Moilanen, E. (2006). Inhibition of classical PKC isoenzymes downregulates STAT1 activation and iNOS expression in LPS-treated murine J774 macrophages. *British Journal of Pharmacology, 147*(7), 790–799. https://doi.org/10.1038/sj.bjp.0706672

Shi, J. D., Bera, K., Mukherjee, P., Alex, A., Chaney, E. J., Spencer-Dene, B., … Boppart, S. A. (2023). Weakly supervised identification and localization of drug fingerprints based on label-free hyperspectral CARS microscopy. *Analytical Chemistry, 95*(29), 10957–10965. https://doi.org/10.1021/acs.analchem.3c00979

Steuwe, C., Patel, I. I., Ul-Hasan, M., Schreiner, A., Boren, J., Brindle, K. M., … Mahajan, S. (2014). CARS based label-free assay for assessment of drugs by monitoring lipid droplets in tumour cells. *Journal of Biophotonics, 7*(11−12), 906–913. https://doi.org/10.1002/jbio.201300110

Syed, R. U., Moni, S. S., Break, M. K. B., Khojali, W. M. A., Jafar, M., Alshammari, M. D., … Mohan, S. (2023). Broccoli: A multi-faceted vegetable for health: An in-depth review of its nutritional attributes, antimicrobial abilities, and anti-inflammatory properties. *Antibiotics, 12*(7). https://doi.org/10.3390/antibiotics12071157. Article 1157.

Tan, Y. Y., Li, J. J., Zhao, G. Y., Huang, K. C., Cardenas, H., Wang, Y. N., … Cheng, J. X. (2022). Metabolic reprogramming from glycolysis to fatty acid uptake and beta-oxidation in platinum-resistant cancer cells. *Nature. Communications, 13*(1). https://doi.org/10.1038/s41467-022-32101-w. Article 4554.

Turner, M. D., Nedjai, B., Hurst, T., & Pennington, D. J. (2014). Cytokines and chemokines: at the crossroads of cell signalling and inflammatory disease. *Biochimica et Biophysica Acta (BBA) - Molecular Cell Research, 1843*(11), 2563–2582. https://doi.org/10.1016/j.bbamcr.2014.05.014

Yuan, T., Yang, T., Chen, H., Fu, D. L., Hu, Y. Y., Wang, J., … Xie, X. (2019). New insights into oxidative stress and inflammation during diabetes mellitus-accelerated atherosclerosis. *Redox Biology, 20*, 247–260. https://doi.org/10.1016/j.redox.2018.09.025

Yue, S. H., & Cheng, J. X. (2016). Deciphering single cell metabolism by coherent Raman scattering microscopy. *Current Opinion in Chemical Biology, 33*, 46–57. https://doi.org/10.1016/j.cbpa.2016.05.016

Zhang, C., & Boppart, S. A. (2020). Dynamic signatures of lipid droplets as new markers to quantify cellular metabolic changes. *Analytical Chemistry, 92*(24), 15943–15952. https://doi.org/10.1021/acs.analchem.0c03366

Zhang, C., Zhang, D. L., & Cheng, J. X. (2015). Coherent Raman scattering microscopy in biology and medicine. *Annual Review of Biomedical Engineering, 17*, 415–445. https://doi.org/10.1146/annurev-bioeng-071114-040554

Zhang, D., Wang, P., Slipchenko, M. N., & Cheng, J. X. (2014). Fast vibrational imaging of single cells and tissues by stimulated Raman scattering microscopy. *Accounts of Chemical Research, 47*(8), 2282–2290. https://doi.org/10.1021/ar400331q

Zhang, J. J., Wang, N., Wang, H. Y., Zhou, W. T., Xu, X. Y., Zeng, Q., & Chen, X. L. (2022, January). Feasibility demonstration of supercontinuum fiber laser-based coherent anti-stokes Raman scattering microscopy. In *Advanced Chemical Microscopy for Life Science and Translational Medicine, Electr Network*. https://doi.org/10.1117/12.2608358